THE GREAT WORLD OF NANOTECHNOLOGY

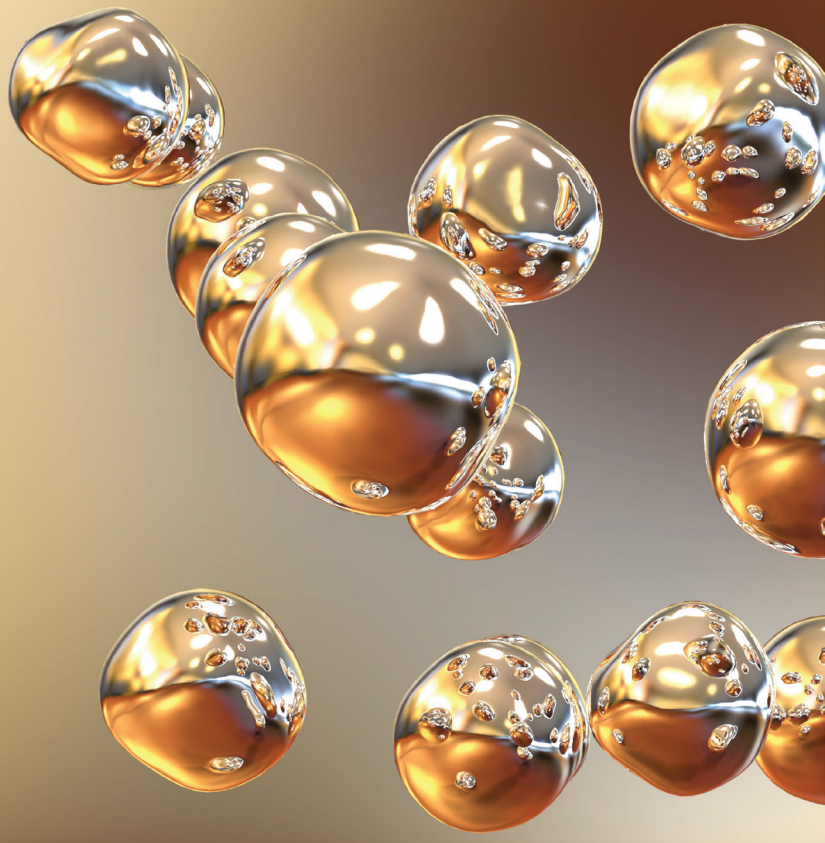

Marcos Augusto de Lima Nobre

(Organizador)

VOL II

EDITORA ARTEMIS
2021

THE GREAT WORLD OF NANOTECHNOLOGY

Marcos Augusto de Lima Nobre

(Organizador)

VOL II

EDITORA ARTEMIS
2021

Editora Chefe Profª Drª Antonella Carvalho de Oliveira
Editora Executiva M.ª Viviane Carvalho Mocellin
Direção de Arte M.ª Bruna Bejarano
Diagramação Elisangela Abreu
Organizadoras Prof. Dr. Marcos Augusto de Lima Nobre
Imagem da Capa Kateryna Kon
Bibliotecário Maurício Amormino Júnior – CRB6/2422

Editora Artemis
Curitiba-PR Brasil
www.editoraartemis.com.br
e-mail:publicar@editoraartemis.com.br

Dados Internacionais de Catalogação na Publicação (CIP)
(eDOC BRASIL, Belo Horizonte/MG)

G786 The great world of nanotechnology [livro eletrônico] : vol. II /
Organizador Marcos Augusto de Lima Nobre. – Curitiba, PR: Artemis, 2021.

Formato: PDF
Requisitos de sistema: Adobe Acrobat Reader
Modo de acesso: World Wide Web
Inclui bibliografia
Edição bilíngue
ISBN 978-65-87396-36-1
DOI 10.37572/EdArt_300621361

1. Nanociência. 2. Nanotecnologia. I. Nobre, Marcos Augusto Lima.

CDD 620.5

Elaborado por Maurício Amormino Júnior – CRB6/2422

EDITORA ARTEMIS
2021

Editora Artemis
Curitiba-PR Brasil
www.editoraartemis.com.br
e-mail:publicar@editoraartemis.com.br

PREFACE

The insertion of new and enhanced materials based on materials belonging to the Nano scale in the day-by-day has growth up in a silent way. In part, a number of works in the nanotechnology stemming of theoretical research using Density Functional Theory (DFT) and sophisticated simulation methods; another part is associated to the protected technologies associated to the military and patented nanomaterial and its process. In this sense, open access to recent aspects on the nanostructures application and properties can be reached in this book. Here, an interesting set of chapters gives opportunity of access texts that reach process and processing of nanostructures, applications of nanotechnology, advanced techniques to theoretical development. A broad set of nanostructures are here covered such as, nanocrystal, superficial nanograins, inner microstructures with nanograins, nanoaggregates, nanoshells, nanotubes, nanoflowers, nanoroad, nanosheets, Also, reveals new investigations areas as grainboundary of nanograins in ceramics and metals. A great number of software has been used as a tool of development of Science and Technologies for nanotechnology COMSOL Multiphysics 5.2. Phenomena and properties has been investigated by recent or classical techniques of materials characterization as Localized Surface Plasmon Resonance (LSPR), X-ray photoelectron spectroscopy (XPS), Field Emission Gun Scanning Electron Microscopy (FEG-SEM) with Energy Dispersive Spectroscopy (EDS), Raman Scattering Spectroscopy (RSS), X ray diffraction (XRD), ^{57}Fe Mössbauer spectroscopy, UV-vis spectroscopy, dynamic light scattering (DLS), Atomic Force Microscopy (AFM), and Field Emission Gun Scanning Electron Microscopy (FEG-SEM). In this sense, collections of spectra from Mössbauer spectroscopy, UV-vis spectroscopy and Infrared spectroscopy can be found. As a matter of fact, some chapter's item can be seemed as specific protocols for synthesis, preparations and measurements in the nanotechnology.

I hope you enjoy your reading.

Prof. Dr. Marcos Augusto Lima Nobre

TABLE OF CONTENTS

CHAPTER 4

CONFINED WATER CHEMISTRY: THE CASE OF NANOCHANNELS GOLD OXIDATION

Data de submissão: 10/05/2021
Data de aceite: 28/05/2021

André Mourão Batista
Universidade Federal do ABC
Programa de Pós-Graduação em Nanociências e Materiais Avançados
Santo André/SP.
http://lattes.cnpq.br/6371655865302362

Herculano da Silva Martinho
Universidade Federal do ABC
Departamento de Física - Santo André/SP.
http://lattes.cnpq.br/6880602655569729

ABSTRACT: Confined and interstitial water have a key role in several chemical, physical and biological processes. It is remarkable that many aspects of water behavior in this regime (e.g., chemical reactivity) remain obscure and unaddressed. In particular for gold surfaces, results from simulations indicated that the first wetting layer would present hydrophilic behavior in contrast to the overall hydrophobic character of the bulk water on this surface. In the present work we investigate the properties of confined water on Au <111> nanochannels. Our findings, based on a large set of morphological, structural, and spectroscopical experimental data and ab-initio computer simulations strongly supports the hypothesis of hydrophilicity of the first wetting layer of Au <111> surface. A unique oxidation process was also observed in the nanochannels driven by confined water. Our findings indicated that the oxidation product is Au $(OH)_3$. Therefore, the Au surface reactivity against confined water needs to be considered for nanoscopic applications as, e.g., catalysis in fine chemicals, pharmaceuticals, and the food industry green processes.
KEYWORDS: Nanolithography. Confined water. Oxidation.

1 INTRODUCTION

1.1 CONFINED WATER

It is well-known that the distinction between gas and liquid disappears above its critical point. (Ferreira et al., 2015) At pressure and temperature above this point, the system becomes a supercritical fluid (McMillan; Stanley, 2010). Supercritical fluids are recognized as possessing unique solvation properties that make them important technological materials (McMillan; Stanley, 2010). Of particular interest is the behavior of water in confined spaces. For example, it plays a key role in protein hydration since nanoscale fluctuations associated with the so-called Widom line can influence biological processes (Chu et al., 2009; Frenkel, 2002).

In fact, confined and interfacial water is very important in chemical, physical, and biological processes. However, many of its properties in confinement remain unanswered. For this reason, it is relevant to probe how geometric confinements and surface interactions affect the properties of bulk water as well as the substrates containing it. (Brovchenko; Oleinikova, 2008; Swenson, 2004) In general, water is not in its bulk form, it is often bound to some substrates, or filling small cavities. Like, for example, water in porous media, as if it were in rocky interstices, and also water as biological material inside cells or bound to the surface of macromolecules and membranes. This is what is defined as confined waters. (Castrillón et al., 2009) Understanding the behavior of confined water at the nanoscale is also relevant to the very important problem of protein stability, transport in ion channels, nano-fluid devices and the thermodynamics of colloidal assemblies (Coudert et al., 2009). This fact highlights the relevance of advancing the understanding of the chemical reactivity of water in contact with these metals, a fact that goes far beyond direct applications in corrosion processes in industry and in transformation processes.

Therefore, several studies have been carried out to investigate the structure and dynamics of water in diverse systems such as biological environments, (Berntsen et al., 2005) nanoporous silica matrices, (Liu et al., 2005; Faraone et al., 2004) vermiculites, (Bergman; Swenson, 2000) molecular sieves, (Swenson et al., 2005) and organic coatings (Philippe et al., 2004).

Proteins, in particular, have many of their properties governed by interactions with water (Raschke, 2006). This, for example, establishes and shapes the panorama of free energy that governs the activity, structure, stability and tertiary and quaternary structures of proteins (Halle, 2004). In fact, a certain amount of water is necessary for the biological activity of all proteins. Even apparently dry enzymes in the presence of gaseous substrates do not show activity in the absence of water (Lind et al., 2004). This intriguing evidence depends on how the water molecules arrange themselves on the molecular scale. Thus, the explicit inclusion of water is essential in solving many biochemical problems. In addition, water, between molecular surfaces, induces different behaviors than those observed in bulk water (Steitz et al., 2003; Jensen et al., 2003; Schwendel et al., 2003), although there is no consensus in this aspect (Yaminsky; Ohnishi, 2003).

1.2 NANOLITHOGRAPHY

This type of manipulation is essential to work in orders of magnitude around 100 nm (Bitton; Frydman, 2006; Binnig et al., 1999). Currently, several studies related to nanolithography are being developed, including local oxidation of silicon and metal surfaces (Edwards et al., 2020; Kim et al., 2020; Chau et al., 2019). Nanolithography via

Atomic Force Microscopy (AFM) has the ability to move a probe over a specific sample surface in a controlled manner, by controlling this applied normal force (Fn) between the probe and the sample surface, thus forming silicon channels (Jirlèn et al., 2017), oxides (Melgarejo et al., 2020), polymers (Stoica; Barzic; Hulubei, 2017), magnetic materials and semiconductors (Celano, 2019).

For making the channels on a Si surface, an AFM tip with high wear resistance is required. Thus, Ogino et al. (Ogino; Nishimura; Shirakashi, 2008) studied a material capable of better resisting the effects of wear, reaching the conclusion of the use of the diamond, despite being expensive. In this way they developed a film of DLC (Diamond-Like Carbon), to coat the tip that is used conventionally of Si_3N_4. The DLC film is an amorphous film with high hardness, high modulus of elasticity, low coefficient of friction and wear, and good tribological properties, being cheaper than a solid diamond tip. (Huang; Jeng; Liu, 2007) In nanolithography, the AFM tip acts as a cutting tool to remove nanoscale materials from the sample to create different types of grooves or trenches. The groove geometry is normally controlled by the normal applied force (Fn) of the applied tip through deflection of the AFM cantilever. To form desired scratched profiles, the grooves can be overlapped by repeated stripes, forming two- and three-dimensional structures, by different repetition and overlapping techniques.

1.3 METALS AND OXIDATION

Metals and metal ions are important inorganic cofactors for biological activity (Berg, 1994). In addition, it is estimated that approximately half of all known proteins contain a metal and that half of that amount only performs its function due to its presence Thomson; Gray, 1998; Waldron; Robinson, 2009). These are called metalloproteinases, which perform several functions in cells, such as storage and transport of proteins, enzymes and signal transducer proteins as well as the important role in infectious diseases (Carver, 2013). As examples we can mention the role of Fe^{+2} / Fe^{+3} ions in the transport of oxygen via hemoglobin (Hsia, 1998) and Cu^{+2} / Cu^{+3} ions in the superoxide dismutase enzyme (Kitajima et al., 1992). The action of these metal ions always occurs in an aqueous medium, where in general the water is in a confined regime.

In particular, some works addressed the issue of corrosion processes and metal reactivity under the action of confined water. Azmat et al. (Azmat et al., 2011) investigated the corrosion of Zn surfaces due to acidified droplets (diameter ~ 0.1 – 5 μm). They concluded that the process is dependent on the initial volume of aerosols, oxygen diffusion, surface area to volume ratio and likely the micro-structural features of the underlying metal. Xia et al. (Xia et al., 2006) investigated the corrosion characteristics of micro and nano-particles

of Cu in distilled water by measuring the absorbance and structure of corrosion products using X-Ray Diffraction (XRD) and Scanning Electron Microscopy (SEM). They concluded that corrosion products of micro-particles increase slowly with increasing immersion time. However, for Cu nano-particles its products increase rapidly with increasing immersion time. Liu et al. (Liu, 2013) investigated the de-hydrogenation on the oxygen-covered surface for Au <100>. They found that the energy barrier of decomposing water strongly reduces the surface of atomic Au covered with oxygen and the O atom can promote dehydration of the H2O molecule.

These studies have important technological implications. In fact, Au/oxide catalysts are widely used in important processes, such as partial oxidation of hydrocarbons, hydrogenation of unsaturated hydrocarbons and CO oxidation. (Hussain; Shah, 2014; Takei et al., 2010) Investigations have shown that Au provides catalytically active systems, whereas selectivity and re-usability are advantages over non-catalyzed organic transformations. (Shahzad et al., 2017) Schryer et al. (Schryer et al., 1989) reported that these Au catalysts show increasing activity in the presence of water, unlike other traditional metal oxide catalysts.

In fact, the water: Au surface reactivity at nanoscale is a chanllenging issue. In the present paper we investigated the oxidation of Au by confined water at nanochannels of variable dimensions produced by nanolithography. The physical-chemical process occurring in the channels were analyzed by high resolution morphological (atomic force microscopy and scanning electron microscopy), structural (X-Ray diffraction, nuclear magnetic resonance), molecular spectroscopy (Fourier-Transform infrared absorption, Raman), and elemental analysis (X-Ray photoelectron spectroscopy) techniques. *Ab-initio* density functional calculations were also performed aiming to furnish possible molecular scenarios to interpret the experimental data.

2 MATERIAL AND METHODS

2.1 AU METALLIC THIN FILMS

High purity Au (99.99%) was sputtered and deposited on Si substrate (275 μm thick, <100> orientation, N/P type, from UniversityWafer, Inc.). The Si substrates were cleaned before Au deposition following a three steps sonication washing in:

(i) 50/50 solution of Extran detergent and isopropyl alcohol;

(ii) isopropyl alcohol;

(iii) deionized water.

The washing time in each step was 30 minutes. The deposition was performed on a Leica EM ACE600 sputter coater equipped with quartz crystal for determination of

the thin film layer thickness. The thicknesses of produced films were 10, 50, 100, 302 and 600 nm.

2.2 SPUTTERING

Physical Vapor Deposition (PVD) consists of a group of deposition techniques, which have in common the fact that they allow material transport in the solid state between the target material and the substrate to be coated. The process takes place in a rarefied chamber. Among the main PVD techniques, evaporation and sputtering can be highlighted. Sputtering is a process very similar to thermal evaporation because it takes material from one place to another, but here there is the presence of an inert gas plasma (usually ionized argon) that ejects material from a metallic target by bombarding particles with high energy. The difference consists in a non-heating of the source (Ohring, 2001).

The advantages of this type of deposition in relation to evaporation is the uniformity of the film obtained, more precise control of thickness, control of the properties of the film such as grain structure and step covering, and also the deposition of multi layers with the use of targets. However, the disadvantages are: high cost of the equipment, deposition rate for some materials can be very low, some materials may suffer degradation due to high energy bombardment, and as the process is carried out at higher pressures than evaporation, an incorporation may occur impurities to the deposited film.

Basic Principles

The sputtering process begins with the chamber, already in a vacuum, being filled with inert gas at a low pressure (Petty, 2008). A high voltage electric field is created between the fixture of the part to be covered and a negative electrode (the metal target that serves as an atom donor), the positively charged gas ions are attracted by the negative metal electrode and are accelerated in their direction, transferring their kinetic energy to the metal atoms upon reaching the target, allowing the metal atoms to be ejected and then the substrate to be covered is bombarded by the ejected atoms and is coated with a thin metallic layer (Venables, 2000).

2.3 ATOMIC FORCE MICROSCOPY (AFM)

Atomic Force microscopy has proven to be a very versatile and multifunctional tool with regard to science and technology, since its creation in the 1980s. Many advances in instrument technology have been achieved, even though they still have their side of limitations, such as relatively slow speeds and restricted area (Shinato; Huang; Jin, 2020; Gómez-Varela et al., 2020; Dufrêne et al., 2021).

When considering its advantages and in relation to other related technologies, we have its ultra high capacity for spatial resolution and ultra low forces exerted on the surface (ranging from 10^{-6} to 10^{-11} N) and other unique features, including the cost of equipment, relatively easy operation and control. AFM has emerged as one of the essential technologies in the observation and fabrication of nanometric structures (Tseng; Notargiacomo; Chen, 2005). The AFM along with their techniques derived, as the Kelvin probe microscope and others, became the most important scanning probe microscope. Allowing topographic (3D) imaging of conductive and insulating surfaces with atomic resolution.

Basic Principles

Its principle is based on a scan made by a tip, which is mounted on a system that attaches the cantilever to a spring of the scanner itself. Throughout the scan, the force between the tip and the sample surface is measured by monitoring the deflection of the cantilever. Thus, a topographic image of the sample is obtained by drawing the deflection of the cantilever in relation to its position in the sample. The final topographic image is then reconstructed using the information from the scanned lines. Each measurement point has a well-defined position. The lines superimposed on the topographic image of AFM correspond to the movements of coming and going (called trace and retrace).

However, other relationships between the tip and the sample can be used to ascertain the properties of the sample, the tip or the intermediate medium, these measures are commonly known as “force measures”. In this type of measurement, the sample is moved up and down applying a tension to the piezoelectric translator, on which the sample is mounted, while measuring the deflection obtained in the cantilever. In some AFMs, the tip to which the cantilever is attached is moved by the piezoelectric translator instead of the sample (Butt; Cappella; Kappl, 2005). Tortonese et al. (Tortonese et al., 1991) developed the piezoresistive PET cantilever as an integrated sensor used to monitor the deflection of the cantilever. Since the initial development, the piezoresistive cantilever has been manufactured by other groups and is now available as a commercial product.

The problem of sample roughness is greatly reduced in AFM compared to other surface strength techniques, since the sample only needs to be smooth on a scale comparable to the radius of curvature at the end of the tip. Various materials, such as mica, a silicon or graphite wafer (HOPG) are available with sufficient smoothness over the required areas (Butt; Cappella; Kappl, 2005).

The essence of AFM force measurements today is to study intrinsic surface forces. The interaction between two surfaces in a medium is one of the fundamental issues in colloid and surface science (Suárez et al., 2012).

2.3.1. Nanolithography

In this work the nanolithography and topological characterization was performed on the Agilent AFM / SPM Series 5500 Atomic Force Microscope. Nanolithography was performed under ambient conditions using the vector scanning method. It was employed a DLC-coated Si tip (model 190DLC from BudgetSensors Innovative Solutions Bulgaria Ltd.) for static plowing. (Xie et al., 2006) The patterns were recorded on a 5 μm^2 area. The nanochannels topography was imaged using a conventional Si_3N_4 tip (in contact mode) that has a low spring constant (about 0.02 N / m), in order to avoid local damage.

Next, the surface was covered by glass cover-ship and water confined between the cover-ship and nanochannels. After that the cover-ship was removed and samples preserved on vacuum. Figure 1 summarizes these steps.

Fig. 1 – Schematic representation of the nanolithography on the Au film deposited on 275 μm thick N/P Si substrate and water confinemet in the channels by spreading a droplet on the surface. After preparation, the Au surface was covered with glass coverslip.

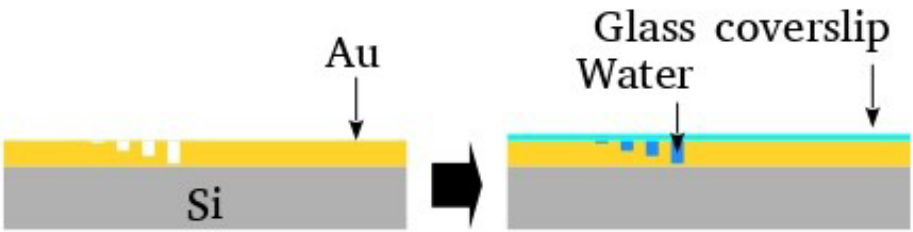

2.4 FOURIER-TRANSFORM INFRARED SPECTROSCOPY (FTIR)

This technique measures the absorption or emission of a given sample, be it solid, liquid or gaseous, in a high spectral resolution simultaneously. Protruding from a dispersive spectrometer, which measures the intensity over a narrow wavelength range separately. The term FT comes from a mathematical process called the Fourier Transform, which converts the raw data into a real spectrum, contributing to an improvement in the signal / noise ratio.

In short, FTIR spectroscopy is a measure of the wavelength and intensity of absorption of IR radiation by a sample, and is widely used in chemical analysis. (Zhang et al., 1995).

Basic Principles

The progression of this spectroscopy, in view of a quantitative analysis, occurs mainly due to the Fourier transform and the new geometries of the spectrometers with the use of Michelson's interferometer, thus making them faster and more effective (Durig; Sullivan, 2016; Eikrem, 1990).

An interferometer mainly consists of a set of mirrors and a beam splitter, transmitting half of the incident radiation from the source to the moving mirror and reflecting the

other half to the fixed mirror. These mirrors reflect the two beams to the divider, where they combine. Therefore, their resulting amplitudes can be constructive or destructive, depending on the divider. In infrared radiation, the sum of all interactions (constructive or destructive) for each component, results in a complex signal called an interferogram.

The Fourier transform spectrophotometer exposes the sample to a single pulse of radiation and response measures. The resulting signal, called biphasic induction, is a direct measure of the temporal coherence of light and contains a rapid decay composed of all possible frequencies. Since the signal measured on the interferometer cannot be interpreted, a mathematical technique called Fourier Transformation is required. This transformation is performed by the computer (software algorithms), presenting the user with the desired information for the spectral analysis (Morgano et al., 2005). The qualitative and quantitative analyzes using spectroscopy in the infrared region have expanded since the data generated by an FTIR spectrophotometer could be digitized, enabling statistical methods to solve chemical analysis problems.

In this work the FTIR spectra was collected using the FTIR spectrometer 640-IR FT-IR coupled to the 610-IR microspectrometer (Varian Inc.) with N_2-cooled Ge detector covering the 600 – 6000 cm^{-1} spectral window. The detection area was 10 × 10 μm^2.

2.5 RAMAN SPECTROSCOPY

Chandrasenkhara Venkata Raman, an Indian scientist who in 1928 studied a phenomenon that was later called Raman scattering, started using this technique. He used sunlight as a source of electromagnetic radiation, a telescope with a collector, and the detector was just his own eyes. Later, more technological sources of excitation were created, such as lasers, which are widely used today (Ferraro; Nakamoto; Brown, 2002). The monochromaticity of radiation from lasers makes it possible to measure with relatively small Raman displacements, considering that the signal obtained in this type of displacement is very low.

The main purpose of this technique is to study the vibrational behavior of the molecules, observing the incident radiation. The Raman spectrum has its intensity in accordance with the Raman displacement. This displacement is due to the difference, in number of waves, between incident radiation and scattered radiation, being called the fingerprint region of a material. And this region has characteristic bands, which give structural and compositional information of the sample (Jenkins; Larsen; Williams, 2005).

Basic Principles

In a succinct description, it can be said that in the inelastic scattering of light, electromagnetic radiation interacts with matter through its electric field (Faria; Santos;

Gonçalves, 1997). Considering that in the Raman effect the transfer of energy depends on the existence of vibrational levels, in this spreading process the interaction of radiation with the network vibrations, initiates the change of the wave vector and the energy of the spread beam in relation to the beam incident (Dove; Dove, 2003).

Scattering can be classified into 3 types of different mechanisms, it is called Rayleigh scattering (or elastic scattering), when energy is preserved between the incident photon and the scattered photon when interacting with the molecule. Therefore, there is no change in the levels of rotational, vibrational or electronic energy in the molecule. As for the non-elastic collision between the photon and the molecule, the photon can be spread with less energy than the incident (Stokes), or with more energy than the incident (anti-Stokes).

In addition to the energy difference in absolute values, the spectrum resulting from non-elastic collisions has significant differences in intensity, since in the anti-Stokes region the intensity of a band is directly proportional to the population of the corresponding vibrational level, which in turn is inversely proportional to the energy needed to populate that level (Faria; Santos; Gonçalves, 1997).

In this work the T64000 Horiba Jobin-Yvon triple Raman spectrometer was used in the subtractive configuration with 1024x256 - OPEN-3LD / R CCD detector for Raman scattering measurements. The excitation laser was the Verdi G5 Laser (Coherent Inc.) operating at 532 nm (green) with a power of 1mW on a 100× objective (laser spot diameter of 1 μm).

2.6 NUCLEAR MAGNETIC RESONANCE (NMR)

Very briefly, Nuclear Magnetic Resonance, like all forms of spectroscopy, is based on the interaction of electromagnetic radiation with matter. However, NMR differs from optical spectroscopy in several fundamental aspects, such as:

i- the separation between energy levels is a result of the interaction of the magnetic moment of an atomic nucleus with an applied magnetic field;

ii- the interaction is with the magnetic component of electromagnetic radiation instead of the electrical component.

In NMR spectroscopy, it is possible to control electromagnetic radiation in the radio frequency (RF) range and describe the interaction of this radiation with the nuclear spins of the system. Thus contributing in part to the evolution of the large number of techniques used in NMR. Almost all chemical elements have at least one isotope with an atomic nucleus that has a magnetic moment, and when it is placed in an external magnetic field, and an excitation is applied with a frequency equal to its precession frequency, that nucleus is removed of your state of balance (Bathista, 2005).

In this work, the NMR experiments were performed with the sample placed inside a 4 mm Zirconia rotor. The control experiments where performed on a silicone greased

Si substrate with the empty rotor as well (i.e., inspecting probe and rotor background). 1H spectra and spin-spin relaxation times (T2) were measured using the spin-echo pulse sequence (π/2 – τ – π – τ – acquisition) conducted in a Varian VNMRS 500 MHz spectrometer operating at the resonance frequencies of 499.8 MHz, with temperature at 25oC. The inter-pulse delay (τ) of the spin-echo pulse sequence was varied from 67 to 4288 μs and 2048 transients were collected. T2 was calculated from the single exponential decay fit of the intensity of the deconvoluted and background-subtracted peaks as a function of 2 τ. The acquisition parameters were π/2 pulse length of 2.5μs and relaxation delay of 5 s. Chemical shifts are reported relative to tetramethylsilane at 0 ppm. The signal was deconvoluted as sum of Lorentz/Gaussian line-shapes.

2.7 SCANNING ELECTRON MICROSCOPY (SEM)

With the technological evolution in the field of sciences as a whole, it requires the researcher to analyze and explain phenomena that occur in nanometric scales. The SEM has excellent resources that allow the observation and characterization of several inorganic and organic materials on this scale (Gomes, 2006). The scanning electron microscope is the most used equipment among the analysis instruments employing electron beams. It has different forms of image acquisition, it has an excellent special resolution, it is easy to prepare samples, it is easy to interpret the images obtained, and it is possible to perform elementary analyzes simultaneously (Zhou et al., 2006).

Basic Principles

The construction of the image takes place through an electron beam that draws the sample, with a point-to-point scanning in two dimensions. The processed signals from the interaction of electrons with the sample are used to amplify a second beam that produces the image on a screen. These signals are originated by the variation in the number of electrons released by the sample in the passage of the beam, which arrive at the detector. The enlargement of the image obtained is achieved by varying the sample size during scanning, reaching up to 1 million times (in current microscopes) (Zhou et al., 2006).

In this work, for morphological characterization was employed the high-resolution field emission scanning electron microscopy model FESEM JSM-6701F (JEOL) in secondary electron image mode and low-vacuum scanning electron microscopy SEM (JSM-6010LA, Jeol).

2.8 X-RAY DIFFRACTION

X-ray diffraction is a physical technique that can be used in several ways, one of which is to identify phases, either for natural or synthetic samples. XRD is well known in the research media, because with it it is possible to identify from peak patterns and their

positions and intensities, by which compounds a determined solid is formed. As these standards are practically unique, a signature for each material can be observed.

Basic Principles

X-rays are a form of electromagnetic radiation that has high energies and short wavelengths – 10 nm to 0.1 nm (Callister; Rethwisch, 2011). It is the main radiation applied in the study of material structures at the level of interatomic distances, that is, of the same order of magnitude as the interplanar spacings of the crystals, so that interference can occur (Padilha, 1997).

One of the main phenomena in wave physics is interference and diffraction. The interference is the result of the coherent superposition of two or more waves from different sources. The interference can be constructive, occurs at points where the displacement difference is equal to an integer number of wavelengths, or destructive, when the path difference is not equal to an integer number of wavelengths.

Diffraction is the phenomenon that occurs when a wave encounters an obstacle or opening of dimensions comparable to the wavelength it spreads and suffers interference. Diffraction is best explained from the Huygens principle, which states that all points on a wavefront can be considered sources of secondary waves that spread in all directions with a speed equal to the wave's propagation speed (Young et al., 2009).

In this work, the crystallographic phase was checked performing the X-ray diffraction experiments at room temperature on a Bruker D-8 Foccus diffractometer (Lynseye 1D detector) with Ni-filtered CuKα1 radiation in range from 30 to 60 (0.02 increment) in θ - 2θ configuration.

2.9 DENSITY DUNCTIONAL CALCULATIONS (DFT)

2.9.1 Molecular dynamics

All the Ab-Initio molecular dynamics (MD) simulations were performed with the CP2K package. (Hohenberg; Kohn, 1964; Hutter et al., 2014) The Gaussian basis set by VandeVondele and Hutter(VandeVondele; Hutter, 2007) derived for use with the analytical dual-space pseudo-potentials proposed by Goedecker, Teter, and Hutter (GTH)(Goedecker; Teter; Hutter, 1996) was used (cuttof of 250 Ry). These pseudo-potentials were used in conjunction with the Gaussian and plane wave (GPW) scheme (Lippert; Parrinello; Michele, 1997) as implemented in the CP2K/QUICKSTEP program. All calculations were performed using the BLYP functional. (Lee; Yang; Parr, 1988) The crystallographic structure for Au obtained from refinement of XRD diffraction as reported by Suh et al. (Suh; Ohta; Waseda, 1988) was used as starting point of calculations. A super-cell of Au crystal was hydrated at

one side (see Results and Discussion section) and then 310 K (Nosé-Hoover thermostat) microcanonical NVE ensemble MD ran up to 100 fs.

2.9.2 Vibrational calculations

DFT (Hohenberg; Kohn, 1964) was used in order to obtain equilibrium geome- tries and harmonic frequencies. Calculations were implemented in the CPMD program using the BLYP functional (Lee; Yang; Parr, 1988) augmented with dispersion corrections for the proper description of van der Waals interactions. (Lee; Yang; Parr, 1988; Lilienfeld et al., 2005) For all simulations, the cutoff energy was considered up to 100 Ry. The linear response for the values of polarization and polar tensors of each atom in the system was calculated to evaluate the eigenvectors of each vibrational mode.

3 RESULTS AND DISCUSSION

The width and depth produced by nanolithography on the surface of silicon coated with gold, as a function of the applied force of the AFM tip are shown in Figure 2 for films with 600 nm of Au layer. Up to 6 μN, the dependence of depth is almost linear (right scale, black symbols). The best fit of data to linear model (black line) furnished intercept of − 31(6) nm and slope of 80(2) nm/μN. Controlling the applied force between 1 − 6 μN we obtained channels with depth of 50 − 500 nm. Otherwise, the values of width of nanochannels present a large dispersion (left scale, red symbols) being almost independent of the tip applied force. On average the width was 388(156) nm. Typical 2D AFM microscopy images before and after pattering for the 600 nm Au layer sample are presented on Supplementary Material section. We also checked the DLC-coated cantilever profile by SEM and we notice that the DLC film remained intact after the patterning process. Otherwise, the homogeneity of channels would be compromised.

Fig. 2 - Depth (left scale, black) and width (right scale, red) of nanochannels as funtion of AFM tip applied force for films with 600 nm of Au. The black line is the best fit to linear model (intercept of -31(6) nm and slope of 80(2) nm/μN).

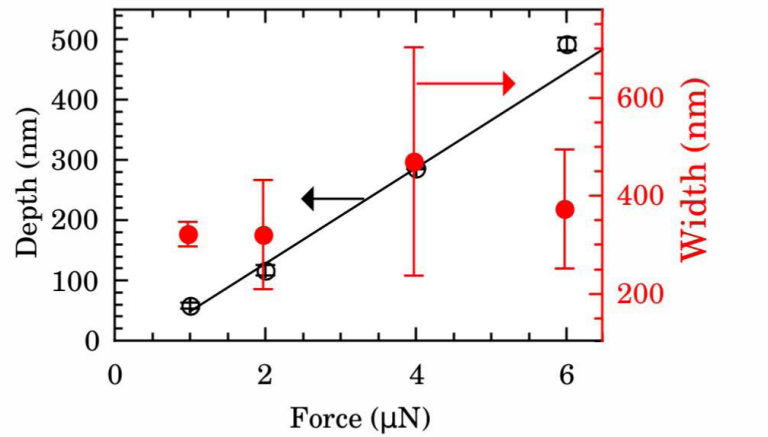

FTIR spectra were taken inside and outside the nanochannels region in order to confirm the presence of water. The spectrum inside the nanochannels region (top of Fig. 3a) presents the typical characteristics water vibrational bands. (Vasylieva et al., 2018) We notice that all these bands presented negligible intensities outside the channels (bottom on Fig. 3a). The broad band from 1300 to 1900 cm^{-1} refers to the bending vibration of the H_2O molecule. (Ludvigsson; Lindgren; Tegenfeldt, 2000; Lucassen; Caspers; Puppels, 200) The band from 3450 to 3950 cm^{-1} refers to the symmetrical and asymmetrical stretch vibration of the O-H bond (WAB), (Ping et al., 2001; Lucassen; Caspers; Puppels, 2000) and the last band from 5150 to 5500 cm^{-1} refers to the inter-molecular hydrogen bonding vibration (WCB). (Kagi et al., 2000; Dickens; Dickens, 1999).

Fig. 3 - a) FTIR spectra showing the presence of water within nanochannels of depth of 245 nm. b) FTIR spectra showing the presence of water even after one week (*) for nanochannels of depth of 115, 245, and 438 nm on a 600 nm Au layer.

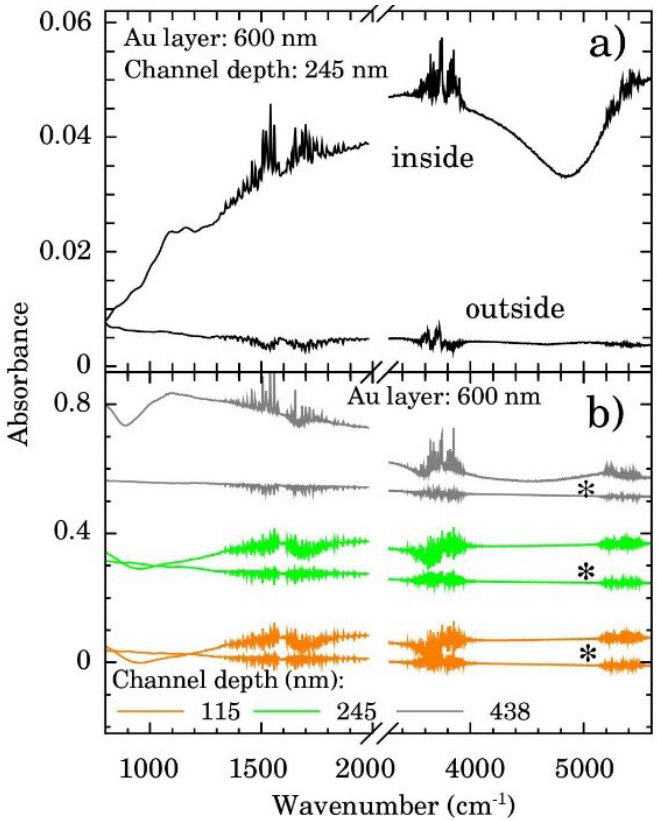

To certify the stability of the containment process, we observed the FTIR signal of the samples after 1 week of vacuum conditioning of the sample. Representative results are displayed on Fig.3b) for samples with nanochannels of depth of 115 nm (orange), 245 nm (green), and 438 nm (gray). The water bands are clearly detectable indicating that it is still present in the confinement region.

The Fig.4 shows the integrated intensities of the OH, WAB and WCB flexion bands after one week in relation to those for fresh samples as a function of the depth of the nanochannels. The relative intensities (and consequently water content) for shallowest samples of depth of 115 nm is almost constant up 1 week. Those of intermediate values of depth (245 nm) presented a intensity decrease of ~ 50% while for the deepest samples (438 nm) water bands intensities after 1 week were ~ 10% of the fresh ones. This finding indicates that confined water is almost bind to the Au surface at shallow samples and these presented higher hydrophilicity compared to the others. It represents an important experimental evidence concerning the hydrophilicity of the first layers of wetting for Au.

Fig. 4 - Relative integrated intensity (1 weak/fresh samples intensities) of OH bending (solid black circle), symmetrical and asymmetrical stretch vibration of the O-H bond (WAB, solid red square), and inter-molecular hydrogen bonding (WCB, solid green diamond) bands.

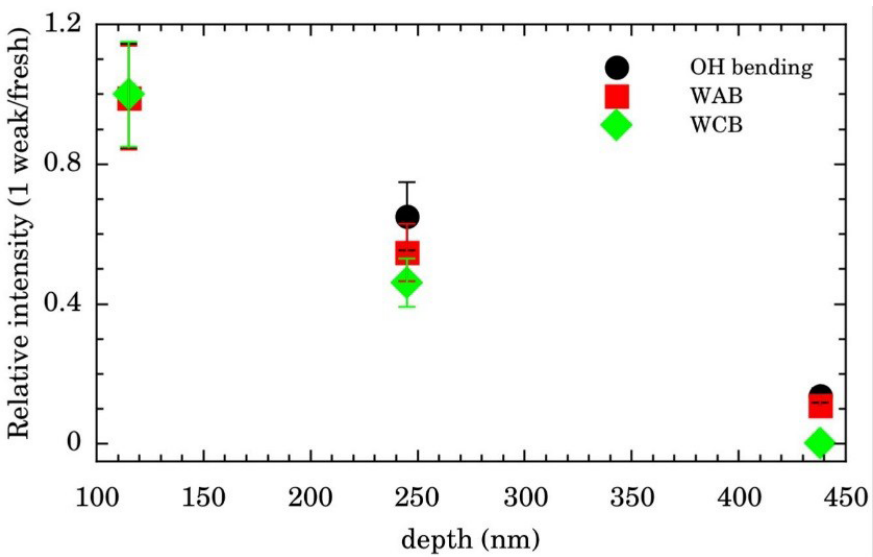

Figure 5a) presents the Raman spectra outside the nanochannels region for samples with Au thickness of 10, 50, 100, 300, and 600 nm. The Si band at ~ 521 cm^{-1} and the 2 th order scattering at ~ 1000 cm^{-1} are observed in all samples. However, it is also observed a strong and broad diffusive electronic Raman scattering for 300 and 600 nm samples. Additional tiny bands appear at 551, 765, and 2334 cm^{-1} (indicated by vertical arrows). These bands are associated to Au-OH stretching mode (Murphy; LaGrange, 1998), e−(H_2O) (Tauber; Mathies, 2002), and OH stretching (Kozlovskaya et al., 2018), respectively. The presence of these bands indicates that some water molecules are adsorbed on the Au surface. This represents another evidence concerning the Au <111> first water wetting layer hydrophilicity.

Fig. 5 - a) Raman spectra of Au thin films (thickness of 600, 300, 100, 50, and 10 nm) deposited over n/p Si and the Si substrate. All spectra were taken outside the nanochannels. Vertical arrows indicate additional Raman bands compared to Si spectrum. b) Representative Raman spectra taken outside (gray), around (red), and inside (blue) the observed oxidation in nanochannels of depth of 115 nm. The inset shows the optical image (100 X objective) in the oxidation region. Asterisks (*) indicates the characteristics oxidation bands at ~ 1602, 2890, and 3260 cm^{-1}.

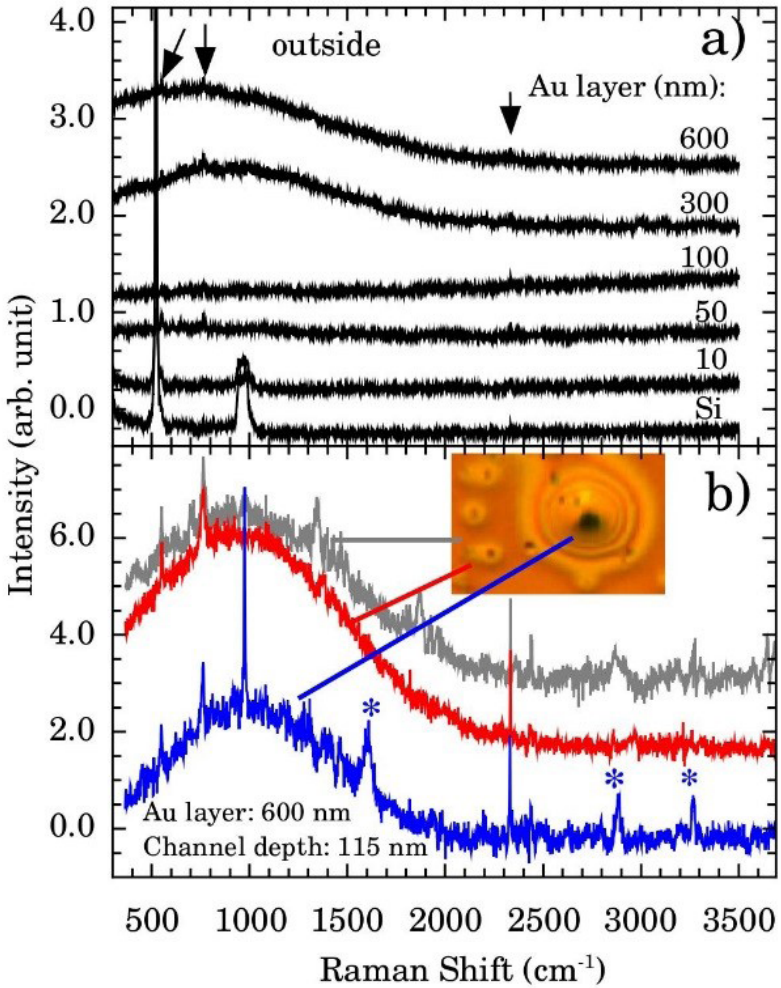

A considerable oxidation process was observed around the nanochannel region (see inset of Fig. 5b). The holes observed in Figure 5b) resembles the “pitting”aspect of corrosion. It is reported that for Au <111> the surface oxidation occurs preferentially by pitting. (Chen; Vesecky; Gewirth, 1992; McCarley; Bard, 1992) We notice that the oxidation corrosion is almost Au-film thickness independent, being observed for 100, 302, and 600 nm films. Figure 5b) shows the Raman spectrum inside, around, and outside of the oxidized region. Bands ~ 2890 and ~ 3260 cm^{-1} are very distinctive in the oxidized region. To the best of our knowledge their assignment are not described in the literature.

Our XRD results (see Fig.6) indicate that the (111) is the preferential orientation on our samples. Reflections from (200) crystal planes are also present but at lower intensities (~ 5%). For comparison, in the fcc Au standard (see inset of Fig.6) the (200) to (111) intensity ratio is ~ 50%. It was performed a symmetrical XRD measurement (θ - 2 θ configuration) the relative greater intensity of (111) reflection indicates that crystallites faces with this orientation predominates on the samples.

Fig. 6 - X-Ray powder diffraction patterns of gold thin films (thickness of 100 nm, 300, and 600 nm) on Si substrate. The inset shows the cubic fcc Au (PDF: 4-784) standard pattern.

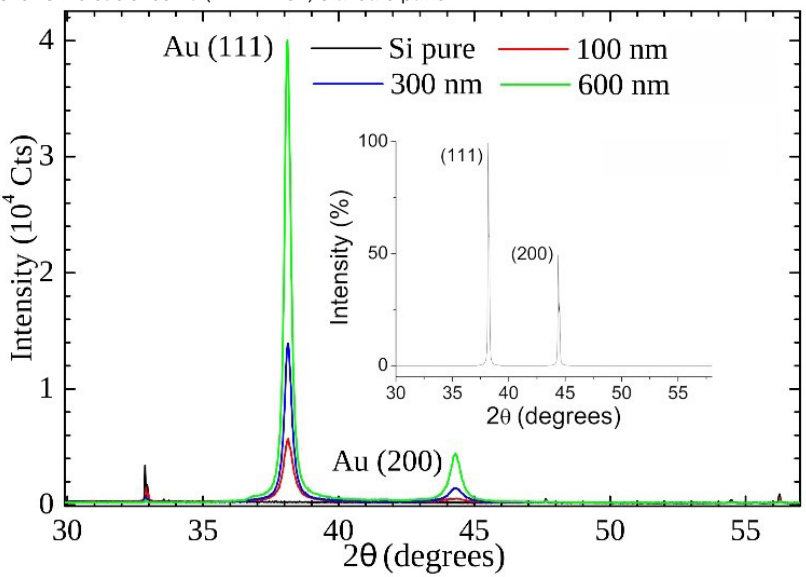

There is still no consensus and much is still being discussed about the coupling of water and gold (Michaelides et al., 2003). Recent experimental studies have shown that the surface of Au < 111> at room temperature is hydrophilic and more stable than other orientations. (Chai; Klein, 2007) Cicero et al. (Cicero et al., 2011) studied the interaction of water layers on the <111> Au surface and the issue of hydrophobicity from ab initio MD simulations. Their results shown that the water/Au interface is hydrophilic due to the charge transfer from oxygen to Au which favours a dynamic attractive coupling between the metal and the first adsorbed water layer. They argue that while oxygen species preferentially reside at the Au <111> sites, hydrogen atoms are evenly distributed around them. Due to the formation of “pitting”, the deposited Au film is unleavened and the potential for local nucleation occurs at the edge of the unevenness. Thus the water at these steps binds more firmly to the Au surface, with a binding energy of 105 meV of the water monomer and the surface of Au <111> (Ibach, 2010). Considering that each water molecule in the bilayer structure is bonded by a half Au - O bond, this means that on Au surfaces the Au - O bond contributes 12 % of the total binding energy per molecule (Ibach, 2010).

Qiang Li et al. (Li et al., 2015) confirmed this theory of the unevenness nucleation point through simulations and previous AFM studies. They concluded that surface and edge defects determine better water adsorption on the Au substrate <111>. They argued that the water clusters had initially been adsorbed to the edges of the Au steps under environmental conditions.

With this information, we started from a hypothesis related to the formation of some type of Au-OH complex performing MD calculations in Au <111> 3 × 3 × 2 super-cell with one face exposed to 67 water molecules. The simulation box had 30 × 35 × 12 nm^3. The water molecules where confined to 12 × 16 × 8 nm^3 (see Fig.7 a). The system found equilibration after 3 fs. Figure 7 b) shows a snapshot of a region close to Au <111> surface. On average there are 6 water molecules bound to the each Au <111> honeycomb (Fig.7 b). Thus the observed Au:O ratio is 1: 3 . Computing the energy of formation of 3 possible structures $(Au(OH)_3)_2$, $(Au(H_2O)_3)_2$, and $H_3Au_3(H_2O)_6$ we found − 302.8 , − 236.2 and − 227.9 eV/atom, respectively. It is possible to conclude that the more stable one is $(Au\ (OH)_3)_2$ which corresponds to $Au(OH)_3$ unit formula. We also performed vibrational calculations on $(Au\ (OH)_3)_2$. From these calculations we were able to assign the 2890 (calculated 2756) and 3260 (calculated 3217) cm −1 bands to out-of-phase (Fig. 7c) and in-phase (Fig. 7d) O-H stretching vibrations, respectively. These results enable us to argue the oxidation product observed in the Au nanochannels under confined water presence is the $Au\ (OH)_3$ complex. This species is usually observed on supported Au-catalytic (see, e.g., ref. (Park; Lee, 1999) and ref. (Takei et al., 2010)).

Fig. 7 - a) Au <111> 3x3x2 supercell including 67 water molecules at one side. The simulation box had 30x35x12 nm^3. b) Snapshot of MD showing the adsorved water molecules around Au <111> honeycomb face. c) and d) Eigenvectors of 2,756 cm^{-1} and 3,217 cm^{-1} vibrations, respectively. Yellow, red, and white spheres represent the Au, O, and H, atoms, respectively.

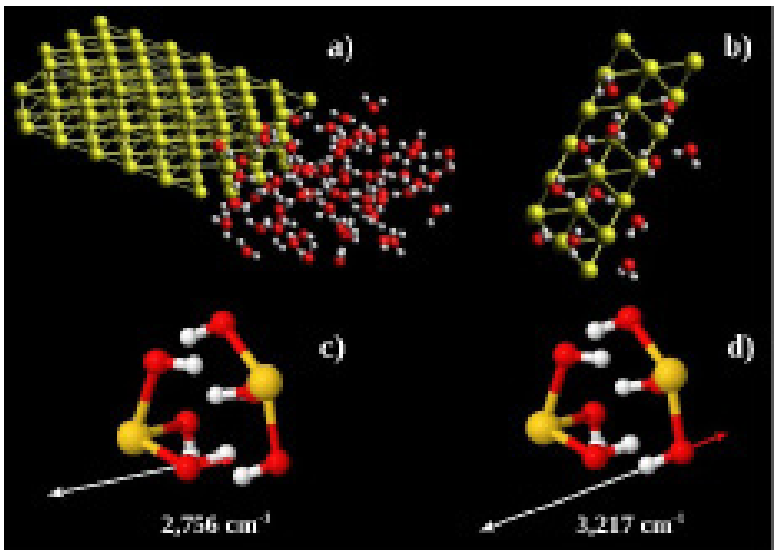

We then performed ^{1}H NMR spin-echo experiments to record the static spectra at different evolution times and to quantify the spin-spin relaxation time, aiming to describe chemical environments and the proton dynamics. However, NMR experiments in films are rarely reported since fast magic angle spinning (MAS) is difficult to implement in this geometry. Static ^{1}H NMR experiments in solid state suffer from strong dipolar coupling and chemical shift anisotropy broadening which results in poorly resolved spectra, unless the species inspected are considerably mobile. As noted below, the spectra obtained are reasonably resolved and the results can be interpreted based on the extensive literature on NMR of Au nanoparticles.

Figure 8 shows the normalized ^{1}H spin-echo spectra of the Au film (600 nm thick) and control experiments as a function of τ. The ^{1}H spin-echo spectra of the sample shows a broad peak around 3.4 ppm. The signal of the sample is more evidenced as the evolution time of the spin-echo is set longer (τ > 1000 μs), as expected, since for longer evolution times the sample inside the rotor is efficiently excited while the probe-background is suppressed.

Fig. 8 - ^{1}H NMR spin-echo spectra of the SiAu sample (600 nm thick) as function of τ. The spectra of the background (empty rotor) and the Si substrate with grease are also shown.

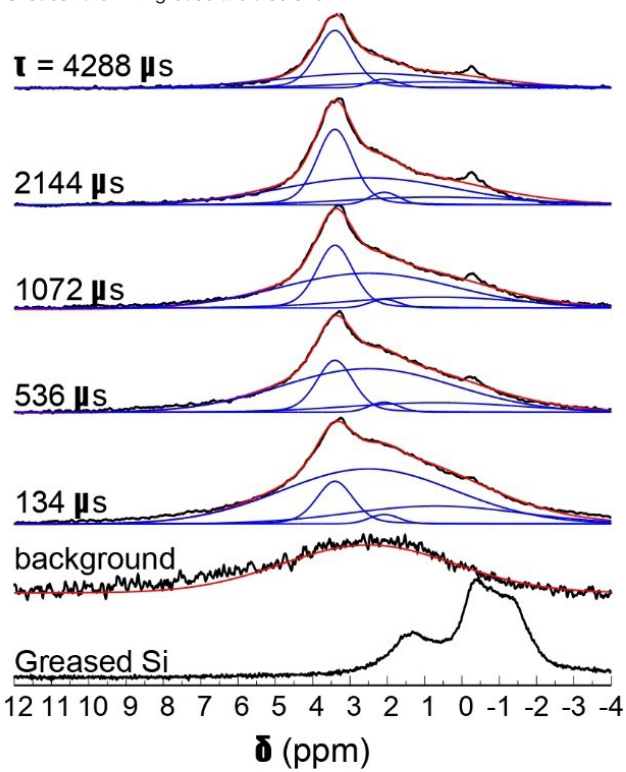

The observed spectra resembles those of amorphous solids with inhomogeneous broadening due to multiple sites and conformations. Each spectrum was carefully

deconvoluted in three peaks and the background, as illustrated in the Figure 8 (see also Supplementary Materials). The most intense peak is at 3.4 ppm (with T 2 of 16 ms), there is a second peak at 2.1 pm (T2 of 7.9 ms), and a broad peak at 0.7 ppm (T2 of 3.6 ms).

The line broadening in this case can be caused by: i) multiple sites and conformations (distribution of chemical shift), ii) chemical shift anisotropy, iii) dipolar coupling, iv) hyperfine coupling of nuclear spins to conduction electrons in the metal (Knight shift), and v) field inhomogeneities caused by variable magnetic susceptibilities around the protons.(Vanderhart; Earl; Garroway, 1981; Alla; Lippmaa, 1982; Sharma et al., 2009; Marbella; Millstone, 2015) The resonance shifts come from some of these features, as the chemical shift, Knight shift and the bulk magnetic susceptibility, which influences the effective local magnetic field.(Vanderhart; Earl; Garroway, 1981; Alla; Lippmaa, 1982; Sharma et al., 2009; Marbella; Millstone, 2015).

We noted that the measurements of the greased Si substrate and the Au covered sample show the silicone grease in the same chemical shift. This illustrates that the Au nanolayer does not contribute significantly to the overall magnetic susceptibility. (Pigliapochi et al., 2019) Possibly, bulk magnetic susceptibility is of secondary relevance in the spectral line broadening and resonance shifts. Furthermore, the importance of the Knight shift in the overall resonance shift and line broadening in ligand grafted Au nanoparticles is long debated. (Badia et al., 1997; Kohlmann et al., 2001) It should be dependent, e.g., on the size and shape of the Au nanolayer or the nanoparticle. More relevant, resonance shifts of the protons in the second or higher coordination to the Au on Au nanoparticles are not remarkably influenced by Knight shifts. For instance, Sharma et al. observed that the ^{1}H NMR of Triphenylphosphine (PPh 3) is observed at 7.3 ppm as free ligand, at 7.5 ppm as.

$Au(PPh)_3$ Cl complex, and at 7.1 ppm as PPh_3-capped gold 1.8 nm nanoparticle. (Sharma et al., 2009) For Tiopronin-capped Au 0.9 nm NPs, Kohlmann et al. found that the methine proton shifts from 3.6 ppm to 4.3-4.7 ppm when Tiopronin is attached to the Au nanoparticles.(Kohlmann et al., 2001) For a series of thiol-terminated-capped Au 1.7 - 4.2 nm NPs,(Hasan; Bethell; Brust, 2002; Schuetze et al., 2016) the ^{1}H downfield shifts of the grafted ligands can be as much as 1 ppm in comparison to the non-grafted ones. Thus, we can restrict our discussion considering that chemical shifts and dipolar interactions are the most important mechanisms influencing the spectral features and relaxation processes.

The first issue to be determined is to confirm the restricted motion of observed protons on the Au surface. Typically, the spin-spin relaxation rates in non-metalic solids are markedly influenced by ^{1}H-^{1}H homonuclear dipolar coupling and dipolar coupling to paramagnetic impurities. (Abragam, 1961; Levitt, 2015) Short T2 imply in strong dipolar coupling that was not averaged out by molecular motion. For instance, ^{1}H T2 of water

decreases from ~ 1 s to 80-240 ms when confined in 50-300 μm microporous glasses. (Taylor; Peterson, 2010; Chencarek et al., 2019) More closely related to our system, for Triphenylphosphine capped Au nanoparticles, T2 of the protons decreases from 5.2 s in the diluted ligand to 40 ms when grafted to the 1.8 nm nanoparticle.(Sharma et al., 2009) T2 of methine protons in tiopronin-capped Au 0.9-1.6 nm NPs has been reported by to be around 156-55 ms.(Kohlmann et al., 2001) These measurements were performed in liquid state, and unfortunately ^{1}H T2 of capped Au nanoparticles in solid state has not been reported (to the best of our knowledge). However, the shortening of T2 in solid state is expected. Thus, we can state that protons in our case are in restricted mobility, and not adsorbed molecules on the surface.

The candidates for the signal around 3.4 ppm are confined water or stable Au-OH complexes, since adsorbed molecules do not contribute to the observed signal. In fact, the ^{1}H NMR shift of adsorbed water is around 4.7-6.0 ppm, (Mogilevsky et al., 2011; Marbella et al., 2014; Osman et al., 2015) which is outside of the observed range. Confined water as monomer or dimer could be observed upfield shifted with respect to bulk water, (Grünberg et al., 2004; Kar; Scheiner, 2004; Osman et al., 2015) around 0.5 - 1.5 ppm, and cannot be ruled out as units contributing to the NMR spectra in that shift range. Another contribution could come from Au-OH complexes, that would be observed around 4.7 ppm, taking into consideration that water as monomer is ~ 3.8 ppm upfield shifted with respect to bulk water(Kar; Scheiner, 2004) while the Au ··· H hydrogen bond would contribute to a 3.5 - 4.1 ppm downfield shift (which is, obviously, a very rough additive estimation taken from quantum chemical calculations).(Kryachko; Remacle, 2005) In summary, it is possible that water monomers or dimers and Au-OH_3 complexes could be existing species but they could only be responsible for small portions of the spectral sidebands (≈ 0.5 - 1.5 ppm and 4-6 ppm).

In order to assign the most characteristic band, centered at 3.4 ppm, we recall that for Au-OH complexes there should be electron donation from the Au to the chemisorbed molecules, (Abraham et al., 2010) similarly to Si-O bonds (to some extent). Remarkable, silanol groups in distinct configurations can be observed as a broad line from 1.8 to 4.5 ppm, the range of the shifts observed here.(Grünberg et al., 2004; Trébosc et al., 2005; Hartmeyer et al., 2007) Furthermore, the static ^{1}H NMR spectrum of MCM-41, with high concentration of surface silanol groups, is very similar to the one observed in our study. (Trébosc et al., 2005) Analogously, hydroxyl of $Zr(OH)_4$ is also observed in this range. (Mogilevsky et al., 2011) Thus, it is likely that the main observed peak around 3.4ppm is due to protons on Au-OH complexes, in agreement with the proposed structures from quantum chemical calculations.

4 CONCLUSIONS

Bearing in mind that water is very important in several chemical, physical and biological processes and that many of its properties in confinement remain unanswered, a fact addressed in the introduction, it is of fundamental importance to understand in more depth how it behaves at the nanoscale, which is where its behavior differs in several aspects from the bulk form (Knight et al., 2019). Its understanding is still much discussed, as there is still no consensus on its reactivity at the nanoscale.

In this work, strong evidence was observed about the hydrophilicity of Au <111> through the relative intensities of the water bands probed by FTIR as a function of the depth of the nanochannels (Fig. 4) and the allocation of small Raman bands (Fig.5). Thus, a unique corrosion process of Au nanochannels exposed to confined water was also observed. Our experimental data pointed out by computer simulations indicated that the oxidation product is Au $(OH)_3$ also supporting the hydrophilicity of the first layer of water wettability over Au. Furthermore, our results indicate an important surface oxidation route that needs to be considered in Au nanosurface applications. An important example is the use of Au in catalysis, since a large amount of organic transformation into fine chemicals, pharmaceuticals and the green processes of the food industry depend on the catalytic activity of Au (see, e.g., ref. (Shahzad et al., 2017)).

REFERENCES

Abragam, A. Thermal relaxation and dynamic polarization in solids. In: The principles of nuclear magnetism.: Clarendon Press, 1961. p. 354–423.

Abraham, A.; Mihaliuk, E.; Kumar, B.; Legleiter, J.; Gullion, T. Solid-state nmr study of cysteine on gold nanoparticles. J. Phys. Chem. C, v. 114, n. 42, p. 18109–18114, 2010. Available on: <https://doi.org/10.1021/jp107112b>.

Alla, M.; Lippmaa, E. Resolution limits in magic-angle rotation nmr spectra of polycrystalline solids. Chem. Phys. Lett., v. 87, n. 1, p. 30 – 33, 1982. ISSN 0009-2614. Available on: <http://www.sciencedirect.com/science/article/pii/0009261482835471>.

Azmat, N.; Ralston, K.; Muddle, B.; Cole, I. Corrosion of zn under fine size aerosols and droplets using inkjet printer deposition and optical profilometry quantification. Corr. sci., Elsevier, v. 53, n. 11, p. 3534–3541, 2011.

Badia, A. et al. Gold-sulfur interactions in alkylthiol self-assembled monolayers formed on gold nanoparticles studied by solid-state nmr. J. Am. Chem. Soc., v. 119, n. 45, p. 11104–11105, 1997. Available on: <https://doi.org/10.1021/ja9726163>.

Bathista, A. Princípios básicos de ressonância magnética nuclear do estado sólido. São Carlos, Brasil, 2005.

Batista, A. M. et al. Gold nanochannels oxidation by confined water. RSC Advances, Royal Society of Chemistry, v. 10, n. 61, p. 36980–36987, 2020.

Berg, J. M. Principles of bioinorganic chemistry.: University Science Books, 1994.

Bergman, R.; Swenson, J. Dynamics of supercooled water in confined geometry. Nature, Nature Publishing Group, v. 403, n. 6767, p. 283–286, 2000.

Berntsen, P.; Bergman, R.; Jansson, H.; Weik, M.; Swenson, J. Dielectric and calorimetric studies of hydrated purple membrane. Biophys. J., Elsevier, v. 89, n. 5, p. 3120–3128, 2005.

Binnig, G. et al. Ultrahigh-density atomic force microscopy data storage with erase capability. Applied Physics Letters, American Institute of Physics, v. 74, n. 9, p. 1329–1331, 1999.

Bitton, L.; Frydman, A. Controllable room-temperature metallic quantum dot. Appl. Phys. Lett., American Institute of Physics, v. 88, n. 11, p. 113113, 2006.

Brovchenko, I.; Oleinikova, A. Interfacial and confined water.: Elsevier, 2008.

Butt, H.-J.; Cappella, B.; Kappl, M. Force measurements with the atomic force microscope: Technique, interpretation and applications. Surface science reports, Elsevier, v. 59, n. 1-6, p. 1–152, 2005.

Callister, W. D.; Rethwisch, D. G. Materials science and engineering.: John wiley & sons NY, 2011. v. 5.

Carver, P. L. Metal ions and infectious diseases. an overview from the clinic. Interrelations between Essential Metal Ions and Human Diseases, Springer, p. 1–28, 2013.

Castrillón, S. R.-V.; Giovambattista, N.; Aksay, I. A.; Debenedetti, P. G. Evolution from surface-influenced to bulk-like dynamics in nanoscopically confined water. J. Phys. Chem.B, ACS Publications, v. 113, n. 23, p. 7973–7976, 2009.

Celano, U. Electrical atomic force microscopy for nanoelectronics.: Springer, 2019.

Chai, L.; Klein, J. Large area, molecularly smooth (0.2 nm rms) gold films for surface forces and other studies. Langmuir, ACS Publications, v. 23, n. 14, p. 7777–7783, 2007.

Chau, Y.-F. C. et al. Fabrication and characterization of a metallic–dielectric nanorod array by nanosphere lithography for plasmonic sensing application. Nanomaterials, Multidisciplinary Digital Publishing Institute, v. 9, n. 12, p. 1691, 2019.

Chen, C. H.; Vesecky, S. M.; Gewirth, A. A. In situ atomic force microscopy of underpotential deposition of silver on gold (111). J. Am. Chem. Soc., ACS Publications, v. 114, n. 2, p. 451–458, 1992.

Chencarek, B. et al. Multi-exponential analysis of water nmr spin–spin relaxation in porosity/permeability-controlled sintered glass. Appl. Magn. Reson., v. 50, n. 1, p. 211–225, Mar 2019. ISSN 1613-7507. Available on: <https://doi.org/10.1007/s00723-018-1050-x>.

Chu, X.-q. et al. Proteins remain soft at lower temperatures under pressure. J. Phys. Chem. B, ACS Publications, v. 113, n. 15, p. 5001–5006, 2009.

Cicero, G.; Calzolari, A.; Corni, S.; Catellani, A. Anomalous wetting layer at the au (111) surface. J. Phys. Chem., ACS Publications, v. 2, n. 20, p. 2582–2586, 2011.

Coudert, F.-X.; Cailliez, F.; Vuilleumier, R.; Fuchs, A. H.; Boutin, A. Water nanodroplets confined in zeolite pores. Faraday Discuss, Royal Society of Chemistry, v. 141, p. 377–398, 2009.

CPMD http://www cpmd.org/ Copyright IBM Corp 1990-2008 Copyright MPI für Festkörperforschung Stuttgart 1997-2019.

Dickens, B.; Dickens, S. H. Estimation of concentration and bonding environment of water dissolved in common solvents using near infrared absorptivity. J. Res. Natl. Inst. Stan., National Institute of Standards and Technology, v. 104, n. 2, p. 173, 1999.

Dove, M. T.; Dove, M. T. Structure and dynamics: an atomic view of materials.: Oxford University Press, 2003. v. 1.

Dufrêne, Y. F.; Viljoen, A.; Mignolet, J.; Mathelié-Guinlet, M. Afm in cellular and molecular microbiology. Cellular Microbiology, John Wiley & Sons, Inc. Chichester, UK, p. e13324–e13324, 2021.

Durig, J.; Sullivan, J. Vibrational spectroscopy, fourier transforms and analytical chemistry. TRAC: Trends in Analytical Chemistry: Volume 9, Elsevier, v. 9, n. 4, p. 104, 2016.

Edwards, C. M.; Ulapane, S. B.; Kamathewatta, N. J.; Ashberry, H. M.; Berrie, C. L. Fabrication and growth control of metal nanostructures through exploration of atomic force microscopy-based patterning and electroless deposition conditions. The Journal of Physical Chemistry C, ACS Publications, v. 124, n. 46, p. 25588–25601, 2020.

Eikrem, L. Process fourier transform infrared spectroscopy. TrAC Trends in Analytical Chemistry, Elsevier, v. 9, n. 4, p. 107–109, 1990.

Faraone, A.; Liu, L.; Mou, C.-Y.; Yen, C.-W.; Chen, S.-H. Fragile-to-strong liquid transition in deeply supercooled confined water. J. Chem. Phys., American Institute of Physics, v. 121, n. 22, p. 10843–10846, 2004.

Faria, D. d.; Santos, L.; Gonçalves, N. Uma demonstração sobre o espalhamento inelástico de luz: repetindo o experimento de raman. Quim. Nova, SciELO Brasil, p. 319–323, 1997.

Ferraro, J.; Nakamoto, K.; Brown, C. Introductory raman spectroscopy (new york: Academic). 2002.

Ferreira, P.; Ishikawa, M.; Kogikoski, S.; Alves, W.; Martinho, H. Relaxation dynamics of deeply supercooled confined water in l, l-diphenylalanine micro/nanotubes. Physical Chemistry Chemical Physics, Royal Society of Chemistry, v. 17, n. 48, p. 32126–32131, 2015.

Frenkel, D. Soft condensed matter. Physica A, Elsevier, v. 313, n. 1, p. 1–31, 2002.

Goedecker, S.; Teter, M.; Hutter, J. Separable dual-space gaussian pseudopotentials. Phys. Rev. B, APS, v. 54, n. 3, p. 1703, 1996.

Gomes, K. K. P. Síntese e caracterização do carbeto de molibdênio nanoestruturado para fins catalíticos na reação de oxidação parcial do metano. Dissertação (Mestrado) – Universidade Federal do Rio Grande do Norte, 2006.

Gómez-Varela, A. I. et al. Simultaneous co-localized super-resolution fluorescence microscopy and atomic force microscopy: combined sim and afm platform for the life sciences. Scientific reports, Nature Publishing Group, v. 10, n. 1, p. 1–10, 2020.

Grünberg, B. et al. Hydrogen bonding of water confined in mesoporous silica mcm-41 and sba-15 studied by 1h solid-state nmr. Chem. Eur. J., v. 10, n. 22, p. 5689–5696, 2004. Available on: <https://chemistry-europe.onlinelibrary.wiley.com/doi/abs/10.1002/chem.200400351>.

Halle, B. Protein hydration dynamics in solution: a critical survey. Philosophical Transactions of the Royal Society of London. Series B: Biological Sciences, The Royal Society, v. 359, n. 1448, p. 1207–1224, 2004.

Hartmeyer, G. et al. Speciation of silanol groups in precipitated silica nanoparticles by 1h mas nmr spectroscopy. J. Phys. Chem. C, v. 111, n. 26, p. 9066–9071, 2007. Available on: <https://doi.org/10.1021/jp071490l>.

Hasan, M.; Bethell, D.; Brust, M. The fate of sulfur-bound hydrogen on formation of self-assembled thiol monolayers on gold: 1h nmr spectroscopic evidence from solutions of gold clusters. J. Am. Chem. Soc., v. 124, n. 7, p. 1132–1133, 2002. PMID: 11841257. Available on: <https://doi.org/10.1021/ja0120577>.

Hohenberg, P.; Kohn, W. Inhomogeneous electron gas. Phys. Rev., APS, v. 136, n. 3B, p. B864, 1964.

Hsia, C. C. Respiratory function of hemoglobin. New England Journal of Medicine, Mass Medical Soc, v. 338, n. 4, p. 239–248, 1998.

Huang, S.-J.; Jeng, Y.-R.; Liu, K.-F. Sliding wear characteristics of the diamond-like carbon films on alloy substrates. Wear, Elsevier, v. 263, n. 7-12, p. 1266–1273, 2007.

Hussain, A.; Shah, S. Mment> computational study of complete methanol dehydrogenation on au (100) and au (310) surfaces: Dominant role of atomic oxygen. Surf. Sci., Elsevier, v. 620, p. 30–37, 2014.

Hutter, J.; Iannuzzi, M.; Schiffmann, F.; VandeVondele, J. cp2k: atomistic simulations of condensed matter systems. Wiley Interdiscip. Rev. Comput. Mol. Sci., Wiley Online Library, v. 4, n. 1, p. 15–25, 2014.

Ibach, H. Vibration spectroscopy of water on stepped gold surfaces. Surf. Sci., Elsevier, v. 604, n. 3-4, p. 377–385, 2010.

Jenkins, A. L.; Larsen, R. A.; Williams, T. B. Characterization of amino acids using raman spectroscopy. Spectrochimica Acta Part A: Molecular and Biomolecular Spectroscopy, Elsevier, v. 61, n. 7, p. 1585–1594, 2005.

Jensen, T. R. et al. Water in contact with extended hydrophobic surfaces: direct evidence of weak dewetting. Physical review letters, APS, v. 90, n. 8, p. 086101, 2003.

Jirlèn, J.; Concina, I.; Lundström, I.; Almqvist, N. Towards nanolithography with starch and α-amylase: Invited lecture. In: European Advanced Materials Congress (EAMC-17), Stockholm, Sweden, 22-24 August 2017. 2017.

Kagi, H. et al. Evidence for ice vi as an inclusion in cuboid diamonds from high pt near infrared spectroscopy. Mineral. Mag., Cambridge University Press, v. 64, n. 6, p. 1089–1097, 2000.

Kar, T.; Scheiner, S. Comparison of cooperativity in ch···o and oh···o hydrogen bonds. J. Phys. Chem. A, v. 108, n. 42, p. 9161–9168, 2004. Available on: <https://doi.org/10.1021/jp048546l>.

Kim, U. S.; Baek, S.-Y.; Kim, T.-W.; Park, J. W. Cold tribo-nanolithography on metallic thin-film surfaces. Journal of nanoscience and nanotechnology, American Scientific Publishers, v. 20, n. 7, p. 4318–4321, 2020.

Kitajima, N. et al. A new model for dioxygen binding in hemocyanin. synthesis, characterization, and molecular structure of the. mu.-. eta. 2:. eta. 2 peroxo dinuclear copper (ii) complexes, [cu (hb (3, 5-r2pz) 3)] 2 (o2)(r= isopropyl and ph). Journal of the American Chemical Society, ACS Publications, v. 114, n. 4, p. 1277–1291, 1992.

Knight, A. W.; Kalugin, N. G.; Coker, E.; Ilgen, A. G. Water properties under nano-scale confinement. Scientific reports, Nature Publishing Group, v. 9, n. 1, p. 1–12, 2019.

Kohlmann, O. et al. Nmr diffusion, relaxation, and spectroscopic studies of water soluble, monolayer-protected gold nanoclusters. J. Phys. Chem. B, v. 105, n. 37, p. 8801–8809, 2001. Available on: <https://doi.org/10.1021/jp011123o>.

Kozlovskaya, E. et al. Raman spectroscopic and theoretical study of liquid and solid water within the spectral region 1600–2300 cm- 1. Spectrochim. ACTA A, Elsevier, v. 196, p. 406–412, 2018.

Kryachko, E.; Remacle, F. Three-gold clusters form nonconventional hydrogen bonds o–h au and n–h au with formamide and formic acid. Chem. Phys. Lett., Elsevier, v. 404, n. 1-3, p. 142–149, 2005.

Lee, C.; Yang, W.; Parr, R. G. Development of the colle-salvetti correlation-energy formula into a functional of the electron density. Phys. Rev. B, APS, v. 37, n. 2, p. 785, 1988.

Levitt, M. H. Relaxation. In:. Spin dynamics: basics of nuclear magnetic resonance. 2. ed.: Wiley, 2015. p. 571–594.

Li, Q.; Song, J.; Besenbacher, F.; Dong, M. Two-dimensional material confined water. Acc. Chem. Res., ACS Publications, v. 48, n. 1, p. 119–127, 2015.

Lilienfeld, O. A. von; Tavernelli, I.; Rothlisberger, U.; Sebastiani, D. Performance of optimized atom-centered potentials for weakly bonded systems using density functional theory. Phys. Rev. B, APS, v. 71, n. 19, p. 195119, 2005.

Lind, P. A.; Daniel, R. M.; Monk, C.; Dunn, R. V. Esterase catalysis of substrate vapour: Biochimica et Biophysica Acta (BBA)-Proteins and Proteomics, Elsevier, v. 1702, n. 1, p. 103–110, 2004.

Lippert, B. G.; Parrinello, J. H.; Michele. A hybrid gaussian and plane wave density functional scheme. Mol. Phys., Taylor & Francis, v. 92, n. 3, p. 477–488, 1997.

Liu, L.; Chen, S.-H.; Faraone, A.; Yen, C.-W.; Mou, C.-Y. Pressure dependence of fragile-to-strong transition and a possible second critical point in supercooled confined water. Phys. Rev. Lett. , APS, v. 95, n. 11, p. 117802, 2005.

Liu, R. Adsorption and dissociation of h2o on au (1 1 1) surface: A dft study. Comput. Theor. Chem., Elsevier, v. 1019, p. 141–145, 2013.

Lucassen, G. W.; Caspers, P. J.; Puppels, G. J. Water content and water profiles in skin measured by ftir and raman spectroscopy. In: International Society for Optics and Photonics. Controlling Tissue Optical Properties: Applications in Clinical Study. 2000. v. 4162, p. 39–45.

Ludvigsson, M.; Lindgren, J.; Tegenfeldt, J. Ftir study of water in cast nafion films. Electrochim. Acta, Elsevier, v. 45, n. 14, p. 2267–2271, 2000.

Marbella, L. E. et al. Gold-cobalt nanoparticle alloys exhibiting tunable compositions, near-infrared emission, and high t2 relaxivity. Adv. Funct. Mater., v. 24, n. 41, p. 6532–6539, 2014. Available on: <https://onlinelibrary.wiley.com/doi/abs/10.1002/adfm.201400988>.

Marbella, L. E.; Millstone, J. E. Nmr techniques for noble metal nanoparticles. Chem. Mater., v. 27, n. 8, p. 2721–2739, 2015. Available on: <https://doi.org/10.1021/cm504809c>.

McCarley, R. L.; Bard, A. J. Surface reactions of gold (111) with aqueous cyanide studied by scanning tunneling microscopy. J. Phys. Chem., ACS Publications, v. 96, n. 18, p. 7410–7416, 1992.

McMillan, P. F.; Stanley, H. E. Fluid phases: Going supercritical. Nature Physics, Nature Publishing Group, v. 6, n. 7, p. 479–480, 2010.

Melgarejo, A.; Schoenek, B.; Zhang, J.; Kim, B. Contact afm nanolithography based on anodic oxidation. Microscopy Today, Cambridge University Press, v. 28, n. 6, p. 12–13, 2020.

Michaelides, A.; Ranea, V.; Andres, P. D.; King, D. General model for water monomer adsorption on close-packed transition and noble metal surfaces. Phys. Rev. Lett. , APS, v. 90, n. 21, p. 216102, 2003.

Mogilevsky, G.; Karwacki, C. J.; Peterson, G. W.; Wagner, G. W. Surface hydroxyl concentration on zr(oh)4 quantified by 1h mas nmr. Chem. Phys. Lett., v. 511, n. 4, p. 384 – 388, 2011. ISSN 0009-2614. Available on: <http: //www.sciencedirect.com/science/article/pii/S0009261411007822>.

Morgano, M. A.; Faria, C. G.; Ferrão, M. F.; Bragagnolo, N.; Ferreira, M. Determinação de proteína em café cru por espectroscopia nir e regressão pls. Food Science and Technology, SciELO Brasil, v. 25, n. 1, p. 25–31, 2005.

Murphy, P.; LaGrange, M. Raman spectroscopy of gold chloro-hydroxy speciation in fluids at ambient temperature and pressure: a re-evaluation of the effects of ph and chloride concentration. Geochim. Cosmochim. Acta, Elsevier, v. 62, n. 21-22, p. 3515–3526, 1998.

Ogino, T.; Nishimura, S.; Shirakashi, J.-i. Scratch nanolithography on si surface using scanning probe microscopy: influence of scanning parameters on groove size. Japanese Journal of Applied Physics, IOP Publishing, v. 47, n. 1S, p. 712, 2008.

Ohring, M. Materials science of thin films.: Elsevier, 2001.

Osman, M. B. et al. Discrimination of surface and bulk structure of crystalline hydroxyapatite nanoparticles by nmr. J. Phys. Chem. C, v. 119, n. 40, p. 23008–23020, 2015. Available on: <https://doi.org/10.1021/acs.jpcc.5b08732>.

Padilha, A. F. Microestrutura e propriedades. São Paulo: Hemus, 1997.

Park, E. D.; Lee, J. S. Effects of pretreatment conditions on co oxidation over supported au catalysts. J. Cat., Elsevier, v. 186, n. 1, p. 1–11, 1999.

Petty, M. C. Molecular electronics: from principles to practice.: John Wiley & Sons, 2008.

Philippe, L.; Sammon, C.; Lyon, S. B.; Yarwood, J. An ftir/atr in situ study of sorption and transport in corrosion protective organic coatings: 1. water sorption and the role of inhibitor anions. Prog. Org., Elsevier, v. 49, n. 4, p. 302–314, 2004.

Pigliapochi, R. et al. When do anisotropic magnetic susceptibilities lead to large nmr shifts? exploring particle shape effects in the battery electrode material lifepo4. J. Am. Chem. Soc., v. 141, n. 33, p. 13089–13100, 2019. PMID: 31271033. Available on:<https://doi.org/10.1021/jacs.9b04674>.

Ping, Z.; Nguyen, Q.; Chen, S.; Zhou, J.; Ding, Y. States of water in different hydrophilic polymers – dsc and ftir studies. Polymer, Elsevier, v. 42, n. 20, p. 8461–8467, 2001.

Raschke, T. M. Water structure and interactions with protein surfaces. Current opinion in structural biology, Elsevier, v. 16, n. 2, p. 152–159, 2006.

Schryer, D. R.; Vannorman, J. D.; Brown, K. G.; Schryer, J. The effects of pretreatment conditions on a pt/sno2 catalyst for the oxidation of co in co2 lasers. NASA-™, v. 103487, p. 19900016993, 1989.

Schuetze, B. et al. Conjugation of thiol-terminated molecules to ultrasmall 2 nm-gold nanoparticles leads to remarkably complex 1h-nmr spectra. J. Mater. Chem. B, The Royal Society of Chemistry, v. 4, p. 2179–2189, 2016. Available on: <http://dx.doi.org/10.1039/C5TB02443A>.

Schwendel, D. et al. Interaction of water with self-assembled monolayers: neutron reflectivity measurements of the water density in the interface region. Langmuir, ACS Publications, v. 19, n. 6, p. 2284–2293, 2003.

Shahzad, S. A.; Sajid, M. A.; Khan, Z. A.; Canseco-Gonzalez, D. Gold catalysis in organic transformations: A review. Synth. Commun., Taylor & Francis, v. 47, n. 8, p. 735–755, 2017.

Sharma, R. et al. Nmr characterization of ligand binding and exchange dynamics in triphenylphosphine-capped gold nanoparticles. J. Phys. Chem. C, v. 113, n. 37, p. 16387–16393, 2009. Available on: <https://doi.org/10.1021/jp905141h>.

Shinato, K. W.; Huang, F.; Jin, Y. Principle and application of atomic force microscopy (afm) for nanoscale investigation of metal corrosion. Corrosion Reviews, De Gruyter, v. 38, n. 5, p. 423–432, 2020.

Steitz, R. et al. Nanobubbles and their precursor layer at the interface of water against a hydrophobic substrate. Langmuir, ACS Publications, v. 19, n. 6, p. 2409–2418, 2003.

Stoica, I.; Barzic, A. I.; Hulubei, C. Fabrication of nanochannels on polyimide films using dynamic plowing lithography. Applied Surface Science, Elsevier, v. 426, p. 307–314, 2017.

Suárez, V. I. T. et al. Sistema de microscopia com multi-pontas: força atômica e campo próximo. Universidade Federal de Alagoas, 2012.

Suh, I.-K.; Ohta, H.; Waseda, Y. High-temperature thermal expansion of six metallic elements measured by dilatation method and x-ray diffraction. J. Mater. Sci., Springer, v. 23, n. 2, p. 757–760, 1988.

Swenson, J. The glass transition and fragility of supercooled confined water. J. Condens. Matter Phys., IOP Publishing, v. 16, n. 45, p. S5317, 2004.

Swenson, J.; Jansson, H.; Howells, W.; Longeville, S. Dynamics of water in a molecular sieve by quasielastic neutron scattering. J. Chen. Phys., American Institute of Physics, v. 122, n. 8, p. 084505, 2005.

Takei, T.; Okuda, I.; Bando, K. K.; Akita, T.; Haruta, M. Gold clusters supported on la (oh) 3 for co oxidation at 193 k. Chem. Phys. Lett., Elsevier, v. 493, n. 4-6, p. 207–211, 2010.

Tauber, M. J.; Mathies, R. A. Resonance raman spectra and vibronic analysis of the aqueous solvated electron. Chem. Phys. Lett., Elsevier, v. 354, n. 5-6, p. 518–526, 2002.

Taylor, R.; Peterson, R. D. Comparison of spin–lattice relaxation measurements made in the presence of strong radiation damping. J. Mol. Struct., v. 970, n. 1, p. 155 – 159, 2010. ISSN 0022-2860. Available on: <http://www.sciencedirect.com/science/article/pii/ S0022286010002140>.

Thomson, A. J.; Gray, H. B. Bio-inorganic chemistry. Current opinion in chemical biology, v. 2, n. 2, p. 155–158, 1998.

Tortonese, M.; Yamada, H.; Barrett, R.; Quate, C. Atomic force microscopy using a piezoresistive cantilever. In: IEEE. TRANSDUCERS'91: 1991 International Conference on Solid-State Sensors and Actuators. Digest of Technical Papers. 1991. p. 448–451.

Trébosc, J.; Wiench, J. W.; Huh, S.; Lin, V. S.-Y.; Pruski, M. Solid-state nmr study of mcm-41-type mesoporous silica nanoparticles. J. Am. Chem. Soc., v. 127, n. 9, p. 3057–3068, 2005. PMID: 15740145. Available on: <https://doi.org/10.1021/ja043567e>.

Tseng, A. A.; Notargiacomo, A.; Chen, T. Nanofabrication by scanning probe microscope lithography: A review. Journal of Vacuum Science & Technology B: Microelectronics and

Nanometer Structures Processing, Measurement, and Phenomena, American Vacuum Society, v. 23, n. 3, p. 877–894, 2005.

Vanderhart, D.; Earl, W. L.; Garroway, A. Resolution in 13c nmr of organic solids using high-power proton decoupling and magic-angle sample spinning. J. Magn. Reson., v. 44, n. 2, p. 361 – 401, 1981. ISSN 0022-2364. Available on: <http://www.sciencedirect.com/science/article/pii/0022236481901785>.

VandeVondele, J.; Hutter, J. Gaussian basis sets for accurate calculations on molecular systems in gas and condensed phases. J. Chem. Phys., American Institute of Physics, v. 127, n. 11, p. 114105, 2007.

Vasylieva, A.; Doroshenko, I.; Vaskivskyi, Y.; Chernolevska, Y.; Pogorelov, V. Ftir study of condensed water structure. J. Mol. Struct., Elsevier, v. 1167, p. 232–238, 2018.

Venables, J. Introduction to surface and thin film processes.: Cambridge University Press, 2000.

Waldron, K. J.; Robinson, N. J. How do bacterial cells ensure that metalloproteins get the correct metal? Nature Reviews Microbiology, Nature Publishing Group, v. 7, n. 1, p. 25–35, 2009.

Xia, X.; Xie, C.; Cai, S.; Yang, Z.; Yang, X. Corrosion characteristics of copper microparticles and copper nanoparticles in distilled water. Corros. Sci., Elsevier, v. 48, n. 12, p. 3924–3932, 2006.

Xie, X. N.; Chung, H.; Sow, C.; Wee, A. Nanoscale materials patterning and engineering by atomic force microscopy nanolithography. Mater. Sci. Eng. R Rep., Elsevier, v. 54, n. 1-2, p. 1–48, 2006.

Yaminsky, V.; Ohnishi, S. Physics of hydrophobic cavities. Langmuir, ACS Publications, v. 19, n. 6, p. 1970–1976, 2003.

Young, C.-C.; Wu, C. H.; Liu, W.-C.; Kuo, J.-T. A higher-order non-hydrostatic σ model for simulating non-linear refraction–diffraction of water waves. Coastal Engineering, Elsevier, v. 56, n. 9, p. 919–930, 2009.

Zhang, Y.-P.; Lewis, R. N.; Hodges, R. S.; McElhaney, R. N. Peptide models of helical hydrophobic transmembrane segments of membrane proteins. 2. differential scanning calorimetric and ftir spectroscopic studies of the interaction of ac-k2-(la) 12-k2-amide with phosphatidylcholine bilayers. Biochemistry, ACS Publications, v. 34, n. 7, p. 2362–2371, 1995.

Zhou, W.; Apkarian, R.; Wang, Z. L.; Joy, D. Fundamentals of scanning electron microscopy (sem). In: Scanning microscopy for nanotechnology.: Springer, 2006. p. 1–40.

ABOUT THE ORGANIZER

MARCOS AUGUSTO DE LIMA NOBRE: Assistant Professor and Researcher (2006 - present), with citation name M. A. L. Nobre, at the São Paulo State University (UNESP), School of Science and Technology, Department of Physics, campus at Presidente Prudente-SP. Head and Founder (2002) of the Laboratory of Functional Composites and Ceramics (LaCCeF acronym in Portuguese, the native idiom), Lab certified by PROPE-UNESP/National Council for Scientific and Technological Development/CNPq*. Grants from National Council for Scientific and Technological Development (CNPq), 2020-2023, 2019-2021 and 2010-2012. Granted with Young-Researcher scholarship by the São Paulo Research Foundation, FAPESP (São Paulo, São Paulo) (2002 - Summer of 2005). Postdoctoral fellow at the Polytechnic School of the University of Sao Paulo (POLI USP-SP) Metallurgy and Materials Science Department with FAPESP Scholarship (1999-summer of 2000). PhD in Science, CAPES Scholarship (Physical Chemistry 1999) by the Chemistry Department, UFSCar-SP. Master in Chemistry CNPq scholarship (Physical Chemistry 1995) by the Chemistry Department, UFSCar-SP. Licentiate degree (4-year of study) in Physics (1993) CNPq and CNPq-Rhae scholarships by the Physics Department, UFSCar-SP. Associate Editor of the Micro & Nano Letters - IET 2019-2020. Associate Editor of the Micro & Nano Letters-Wiley, 2020 - present. Ethycal Editor of the Applied Mathematics Science (Reuse) m-Hikari and Modern Research in Catalysis, Irvine-CA, USA (2017- date). Editorial board member of the Artemis Editora, Brazil. Nowadays, have 02 patents. Has published 80 papers at 39 different indexed Journals of renowned Editors. In May/25/2021, has been cited 1379 times, at 76 papers (47 with citations), in according to the ResearchID actual Publons base having an H-index equal to 23. Academic Google score: H = 28, i10 = 45 and 2338 citations. Reviewer of more than three dozen of journals. Have more than 580 communications and presentation in National and International Congress and Symposiums, from these 150 has been published as Conference Paper. Author or co-author of 20 Chapters of book approaching Scientific Divulgation, Teaching of Physic and Chemistry for teachers actuating in the graduating degree. For this, the Nanoscience and Nanotechnology have been the first strategy. Received tens of National and International Awards, Honorable mentions and distinction mentions, as well as titles. Research skills: Materials Science, Advanced Ceramic Processing, Linear and Non-linear Advanced Dielectrics Materials, Solid state chemistry, Impedance spectroscopy of solids and fluids, Structural Characterization via Mid infrared Spectroscopy with Fast-Fourier-Transformed of solid and fluids, Structural and non-structural Phase Transitions in Semiconductor Ferroelectrics. Also, Molecular Interactions in Functional Fluids as biofuels and its blends, probed via mid infrared Spectroscopy. Research interests: New Functional Materials as

amorphous composite based on carbon/nanoparticles and Semiconductor Ferroelectrics. Member of the Program of Post-Graduation in Chemistry at UNESP - Campus of São José do Rio Preto, IBILCE UNESP – SP, Brazil.

INDEX

G

K

M

N

O

Z

EDITORA
ARTEMIS